Material Properties of 17-4PH Stainless Steel Fabricated by Atomic Diffusion Additive Manufacturing (ADAM)

Nandhini Raju*, [c], Peter Warren*, Ramesh Subramanian†, Ranajay Ghosh*, Seetha Raghavan*, Erik Fernandez* and Jayanta Kapat*

*Department of Mechanical and Aerospace engineering, University of Central Florida, Orlando, FL 32816.
†Siemens Energy Inc, Orlando, FL- 32817.

[c] Corresponding author: nandhini@knights.ucf.edu

Abstract

The objective of this paper is to investigate the material properties of 17-4PH stainless steel printed by the Atomic Diffusion Additive manufacturing technique. Samples with film cooling holes in different orientations were manufactured in a Markforged Metal-X machine. The presence of the holes in these samples helps to understand the printability and accuracy of internal cooling holes, as manufactured by the Metal-X machine. Manufactured samples were first washed to remove the plastic binder. These pre-sintered samples were tested, before sintering, for density, microstructure analysis, CT (Computerized Tomography) scan, roughness, and XRF (X-ray Fluorescence Spectrometer) to understand the material properties. The printed holes, their anomalies, and selection of standards of testing will be discussed along with the material behavior of 17-4PH stainless steel.

Introduction

Additive Manufacturing has been around for nearly 3 decades, and the field has seen a significant amount of research and attention. There are new and innovative printing techniques that are constantly being developed, which leads to more and more materials to be feasibly additively manufactured. While thermoplastics can be printed with ease and with a variety of methods, both ceramics and metallic materials are much more challenging to print accurately, and with the desired material properties [1]. Additive manufacturing provides designers and engineers a great deal of freedom and flexibility during the initial production and prototyping stages of a project. Every new material that can be additively manufactured can help assist a new industry to develop solutions and improvements rapidly and decrease new product time to market. Some of the challenges that metallic additive manufacturing techniques face are the difficulties in modeling the physical phenomena that exist in the process, including melting, vaporization, solidification, heat transfer, chemical reactions, and many other complex processes. The ability to accurately model and predict geometry and material properties of metallic additively manufactured components hinges directly on the gathering of data at all stages of the manufacturing process and exploring the effect of intricate geometries on the printing process [2-3].

Currently, there are many methods to additively manufacture metals, but they have all been developed over the past few decades and are not yet without flaws in production [4]. The methods to print metallic components can be broken down into three main groups: Powder Bed Systems, Powder Feed Systems, and Wire Feed Systems. An example of the powder bed system would be Binder Jet Printing (BJP), and an example of the powder feed system would be Selective Laser Sintering (SLS). The method that we examine in this work will fall under the Wire Feed System category and is referred to as Atomic Diffusion Additive Manufacturing (ADAM). ADAM is a wire feed system and utilizes a solid binder material, as opposed to liquid, to hold the material in a solid wire form before extrusion. The wire feed system has worked very well for thermoplastic materials, but it is a relatively new method for printing metallic components [5].

Literature review

ADAM was developed in 2017 by the company, Markforged [6]. The method utilizes a combination of both metal powder and polymer that is formed into a wire feed system. Because the powders are locked into the polymer binder material, they do not produce any toxic inhalants while being handled. The binder material must be removed during the sintering phase to increase the density of the component, this causes a roughly 20% shrinkage to the part. While the shrinkage is uniform throughout, intricate features in the geometry can cause distortions. This makes the shrinkage difficult to predict for intricate components [7]. There are currently many materials that are produced through this method, and they include stainless steel, titanium alloy, aluminum, and tool steel. The focus of this work is an examination into the manufacturing of the 17-4 stainless steel. Metallic samples which are manufactured via ADAM do exhibit the material properties that are desirable from metallic materials, but like most additive manufacturing methods, the samples also exhibit anisotropic behavior. During mechanical testing of 17-4PH stainless steel, dog bone specimens manufactured via ADAM have demonstrated ellipsoidal stress concentrations in the strain fields [8].

Because of the high melting temperature of metals (typically above 1000°C), at some point during the manufacturing process of any of the techniques, the component must be taken near its melting point for densification of the material [9]. During this sintering process, that material will shrink, and predicting the amount of shrinkage that will occur can be difficult. Modeling and thorough physical understanding of the phenomena that occur during sintering and even before sintering is still lacking [10]. To accurately predict the shrinkage that will occur during the sintering phase, many samples must be made with varying geometries and compared before, during, and after the samples are sintered. With the ongoing development and innovation that is occurring in the field of additive manufacturing, it is critical for researchers to work together to help develop and implement ASTM standards of testing for these parts. Parts made via additive manufacturing must be qualified efficiently.

In this work, we will record data such as density, CT scans, surface imaging, microstructure analysis, and the XRF at the green stage to help assist in the gathering of data to assist in forming a better understanding of the materials at various stages of the manufacturing process [11]. Metallic components are much more difficult to prototype, so the benefits that could be received from the capability of rapid printing and manufacturing of components of a specific geometry would be substantial.

Research Methodology

17-4PH stainless steel specimens were manufactured using a Markforged Metal X machine at The Siemens Energy Innovation center, Orlando. Samples were printed as solid cubes and some of them, with cooling holes. Before sintering (after de-binding) conditions were considered here for material property testing. Samples were tested for XRF (X-Ray Fluorescence Spectrometer), density, roughness, microstructure analysis, and CT (Computerized Tomography) scan to understand the material properties before the sintering processes. Additionally, a detailed conceptual approach was developed and mentioned in fig.1 to understand the material behavior before the sintering stage.

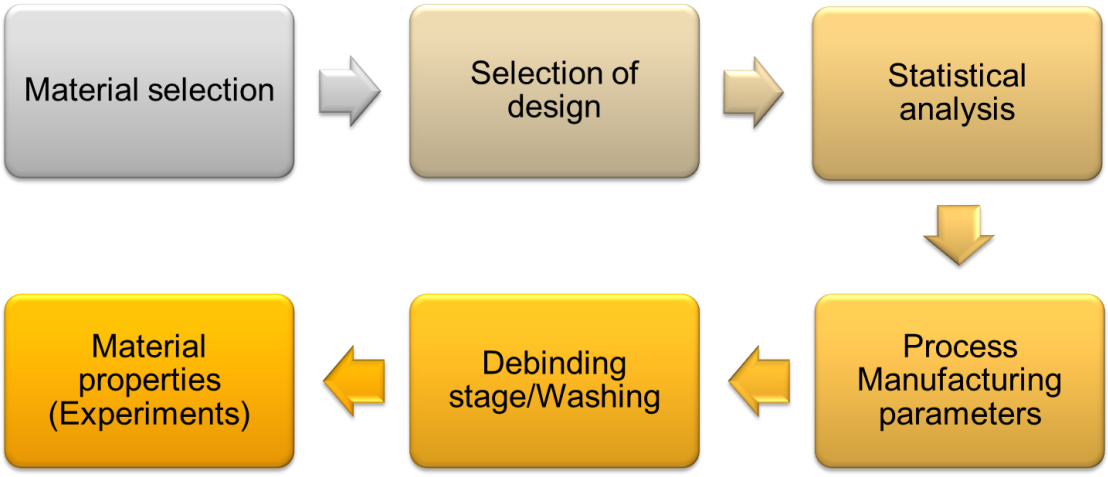

Figure 1 process flow to investigate material at the de-binding stage

According to the process flow, materials are selected based on the requirements or applications. Because the ADAM technique involves binder and metal powder at the printing stage, during the sintering stage, there will be shrinkage which will lead to a dimensional change of the final part. In this research, designs were included specific orientations of cooling holes. Furthermore, statistical analysis was included to perform material property tests at higher confidence intervals. ASTM E122-17[12] standard is used here to decide the sample size. Selection of manufacturing and de-binding parameters were considered before performing material testing. Manufacturing and de-binding parameters are limited to users according to the Markforged machine, but these parameters are included in the process flow.

Experimental Plan

Printing & Parameters

Test article designs were input in the STL format to the machine, with Eiger software providing options to select material and furnace type. Here, design scales can also be changed. For this research, the scale was maintained as 1 and a triangular infill strategy was selected. Wall layers were fixed as 4 mm and layer thickness was maintained as 125 microns. Based on the material and design selection, printing time and wash time can be estimated. For example, to print a 20 mm 17-4PH stainless steel cube, metal X required a 7-hour time for print. Since wire feedstock material consists of a binder and fine powders, most of the binder needs to be removed from the part at this washing stage, before the sintering stage. For this ADAM machine, metal X uses Opteon sion, a chemical solution [13] that is used in the washing basket for the chemical de-binding process. After the de-binding process, parts are ready to sinter at the furnace.

Design

Two solid cubes (20 mm), and cubes with film cooling holes (similar to those used in turbomachinery cooling) were printed in different orientations. For the initial run, a total of 5 samples were printed. Fig.2 shows the design of the samples used for this research.

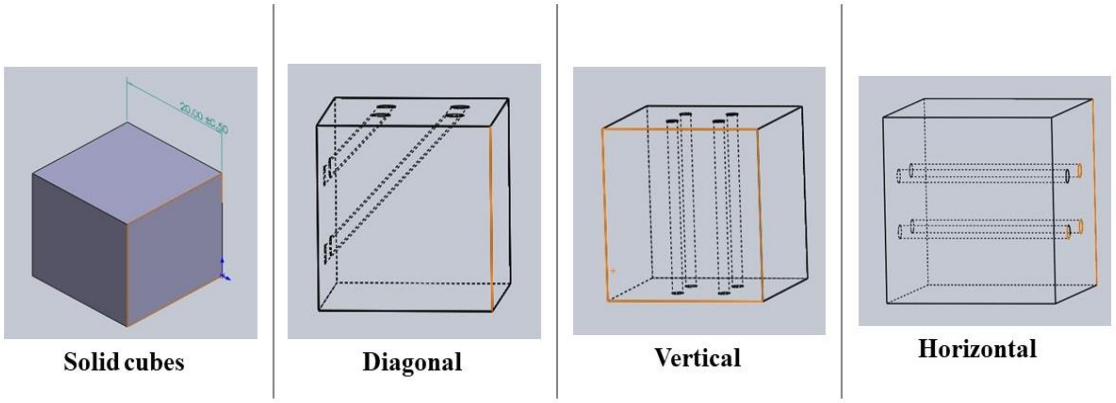

Figure 2 design of the samples printed by Markforged metal X system

Film cooling holes are printed in X(horizontal), Z(vertical), and diagonal directions and are mentioned in fig.2. The main reason is to investigate these holes' accuracy and printability by the ADAM technique.

Testing

Table 1 Experimental campaign for printed samples (before sintering)

Experiments	***XRF***	***Density***	***Roughness***	***Microstructure analysis***	***CT scan***
Quantity	5	2	2	4	4

A total of 5 samples are printed and washed in the bin. Before sintering, these samples were tested for density, roughness, microstructure, CT scan, and XRF. An experimental campaign was designed as mentioned in Table1. These tests provide information more about the material properties of the 17-4PH stainless steel at the pre-sintering stage. Also, the printed samples' dimensions were measured and compared with the original design files.

Results & discussion

Firstly, understanding the chemical composition of the material is important, as it determines the material behavior at any stage of manufacturing. So, a total of 5 printed samples were washed and tested in the PANalytical Epsilon machine to understand the elemental composition. This XRF machine predicts elements from sodium and above with a 50KV silver anode. The result of XRF testing composition of 3d printed 17-4PH stainless steel is mentioned in Table 2.

Table 2 Chemical composition of 17-4PH stainless steel

Composition	***Si***	***P***	***S***	***Cr***	***Mn***	***Fe***	***Ni***	***Cu***	***Nb***
Amount	0.441%	0.209%	240.2ppm	17.273%	0.255%	73.931%	3.878%	3.753%	0.235%

According to table 2, element compositions are mentioned in weight percentage and part per million (ppm). Values are similar as nominal 17-4PH stainless steel, grade 630 as mentioned in the ASTM A693-16 standard [14].

Measurements & density

These printed precipitation-hardening stainless-steel samples were measured to quantify any deviations from the design intent. It was measured as 24.015 mm X 23.801 mm X 23.776 mm in an average of 10 different measurements over every sample. It was designed to print 20 mm. Along with binder addition, before the de-

binding stage, measured dimensions were larger than designed. Note that upon sintering parts will later shrink due to binder burn out, and metal powder sintering. Samples were printed on the sheet with a support plate at the bottom by default. These plates are helpful to maintain uniform thermal gradients in the cube at the sintering stage.

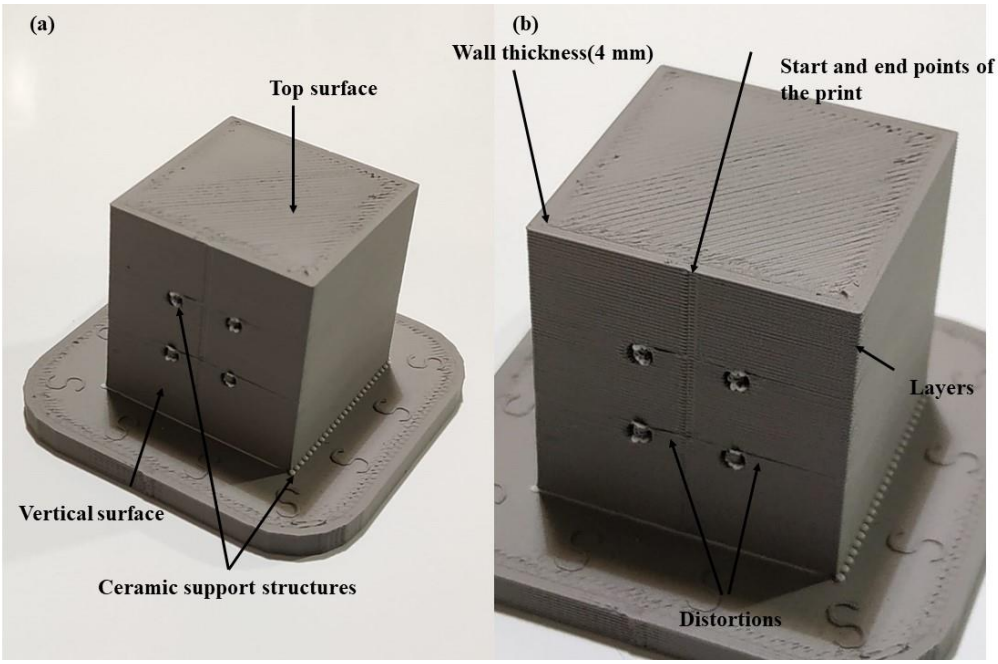

Figure 3(a) Ceramic support structures in the bottom and in the overhang features(holes) (b) start and points, intralayer, and wall thickness

Additionally, the stainless-steel cubes were printed with ceramic support structures per the ADAM technique, as can be seen in fig.3. After sintering, ceramic features can be removed from overhang structures, and the bottom easily. In fig.3(a) and 3(b) ceramic support structures, start, and endpoints are mentioned. The start and endpoints of the print are visible, and distortion around the cooling hole geometry can be observed. Measured samples were further tested for density according to ASTM B311- 17[15]. It was measured as 1.804 g/cm^3. The main reason for this lower density compared to the nominal value is the presence of a triangular infill instead of a solid infill. Also, it has inherent porosity provided with metal powders not tightly packed in the cube.

Roughness

Roughness analysis was performed at CREOL (The College of Optics and Photonics), UCF. A Dektak XT profilometer was used for measuring surface profile and roughness. Here, the top surface of the sample was considered for testing, with two samples tested for roughness. The stylus of the machine was placed over the top surface of the sample in the x and y direction as mentioned in fig.4(a).

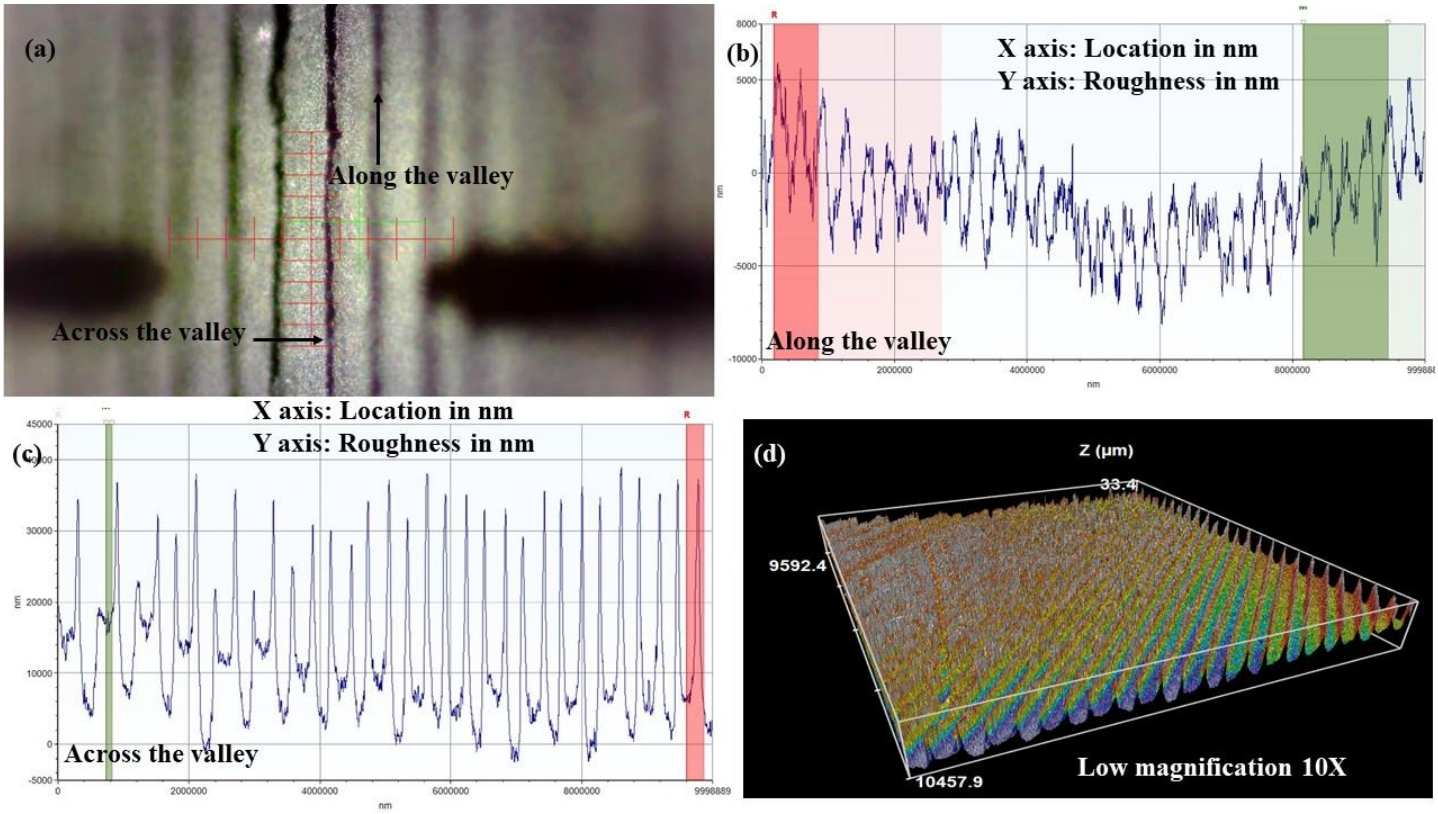

Figure 4(a) location of the stylus over the top surface. (b) Roughness profile along the valley (c) Roughness profile across the valley. (d) Roughness 3D profile

In fig 4(a), the location of the stylus over the top surface of the solid cube is shown. The stylus runs along with the printed layer that is named "along the valley", and in the opposite direction mentioned as "across the valley" (fig.4(a)). Along the valley (fig. 4(b)), printed samples were measured as 1.9 microns and 1.55 microns for two printed samples. Similarly, across the valley (fig. 4(c)), printed samples measured as 12 microns and 9.3 microns for two printed solid cubes. Across the valley, samples were produced with more patterned waviness comparing the results along the valley. Results derived from the Dektak profilometer were 2d profiles over the selected surface area. To produce the 3D roughness profile with low magnification 10X, a Sensofar SNeox 90 metrology equipment at Siemens Energy. Measurements were done according to ISO 25178[16] and provided a 3d color map along with an average "Sa" value of 7.7813 microns for the overall top surface of the sample. This surface roughness profile is mentioned in fig 4(d).

Microstructure analysis

To understand the feedstock, formation of layers, and defects, the JEOL-6480SEM machine was used at AMPAC (Advanced Materials Processing and Analysis Center), UCF. To investigate the valleys for microstructure analysis, printed materials were not polished. Microstructure analysis results are mentioned in fig. 5.

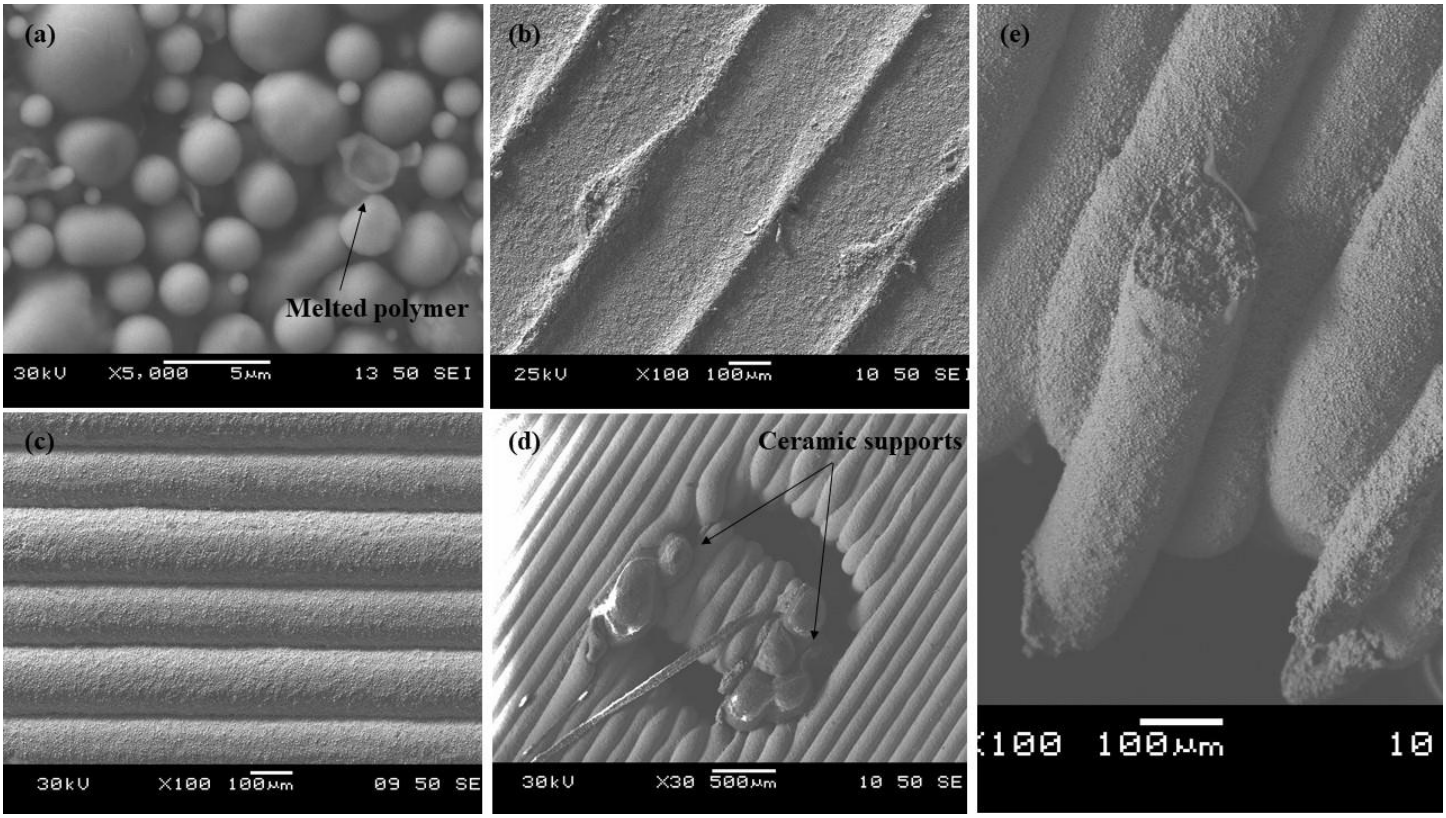

Figure 5(a) metal powder encased with plastic binder (b) microstructure analysis over the top surface of the sample. (c) microstructure analysis of the vertical surface (d) film cooling holes (horizontal) and ceramic supports (e)distortions near the film cooling hole

Metal wire feedstock was analyzed and shown in fig.5a. Metal powders encased in melted polymer binder were observed. Overall metal powders were spherical with less irregular shapes. These metal wire feedstocks were used in the Markforged metal X machine to print the samples. The top surface and vertical surface of the printed samples were examined here for analysis. According to solid cubes, there were fewer distortions observed in the top and vertical surface (fig. 4(b), (c)). Regions near the cooling hole geometry show visible distortions; holes were printed in near-circular shapes with visible layer depositions. These distortions are observed at the hole area where printed layers were discontinued.

Particle size analysis

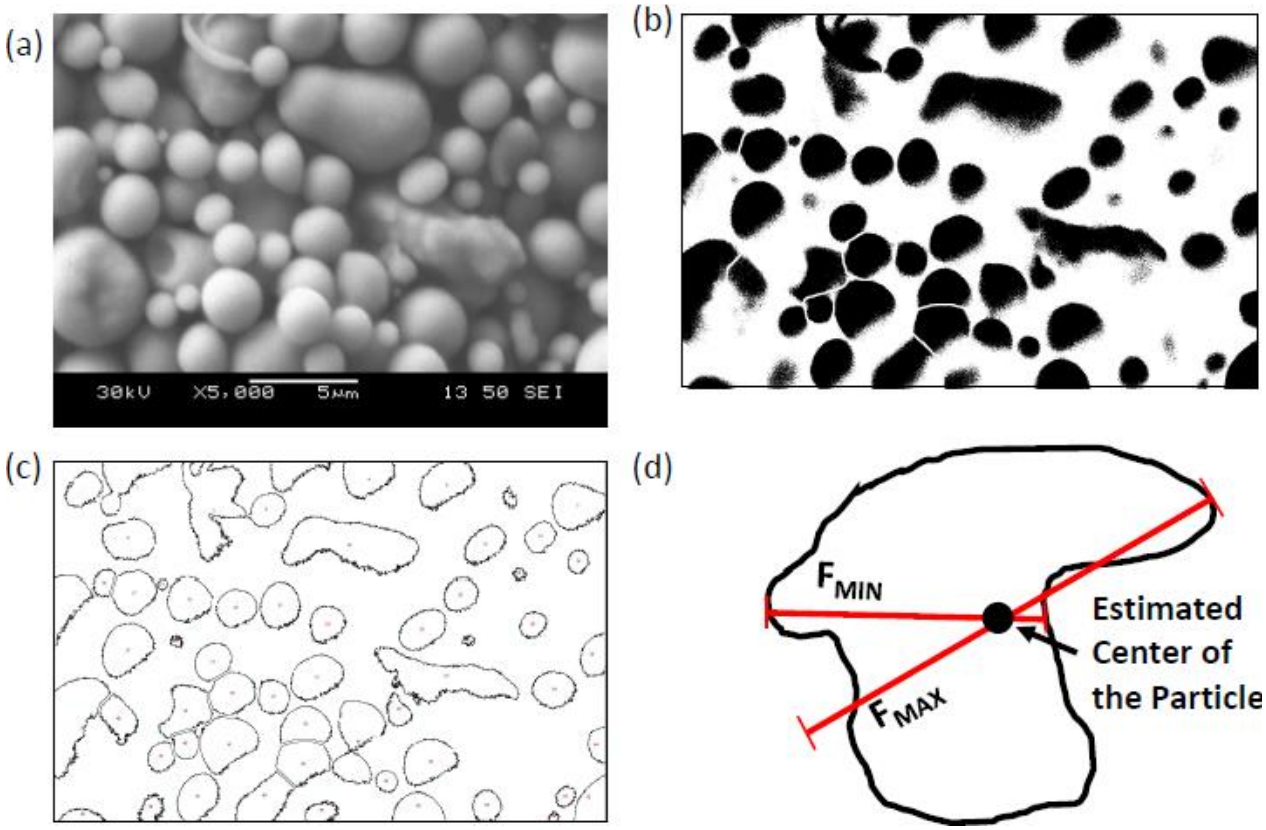

Figure 6 Estimation of the average particle size using ImageJ software. a) SEM image of the green part which shows the particles. b) All pixels are sorted to either black or white (1 or 0) to indicate whether a particle is present or not. c) The outline of each particle is shown. d) Illustration of the Feret's diameter calculation for abnormal particle shape, to determine particle size

The average particle size of the green part was gathered from SEM images. An image processing software called "ImageJ" was used to organize the pixels in a way that the particle area and diameters could be calculated [17]. The average particle size was calculated as shown in fig 6. First, an SEM image was taken, for this work, we used a total of 10 images from 5 green parts. Next, ImageJ can sort the pixels of the images into either black or white, which was represented in the program as a 1 or 0. Next, the perimeter of each particle was determined, this also led to a calculation of the number of particles within the image. Finally, to calculate the diameter of the particles, Feret's diameter is utilized. Feret's diameter is a method to calculate the diameter of a particle that is not a perfect circle which is mentioned in fig.6 [18]. Feret's diameter has also been referred to as the caliper diameter. The formula works by averaging the diameter in at least two orientations. If only two orientations are used, the max and min should be used, however with software, many orientations can be averaged in for a more accurate answer. The average particle size for the measurements taken from this work is 2.58 microns with a standard deviation of 1.23 microns. There is room for error during post-processing with ImageJ, as some of the particles in contact with one another may be considered as one particle, and then filtered out due to being oversized.

CT scan

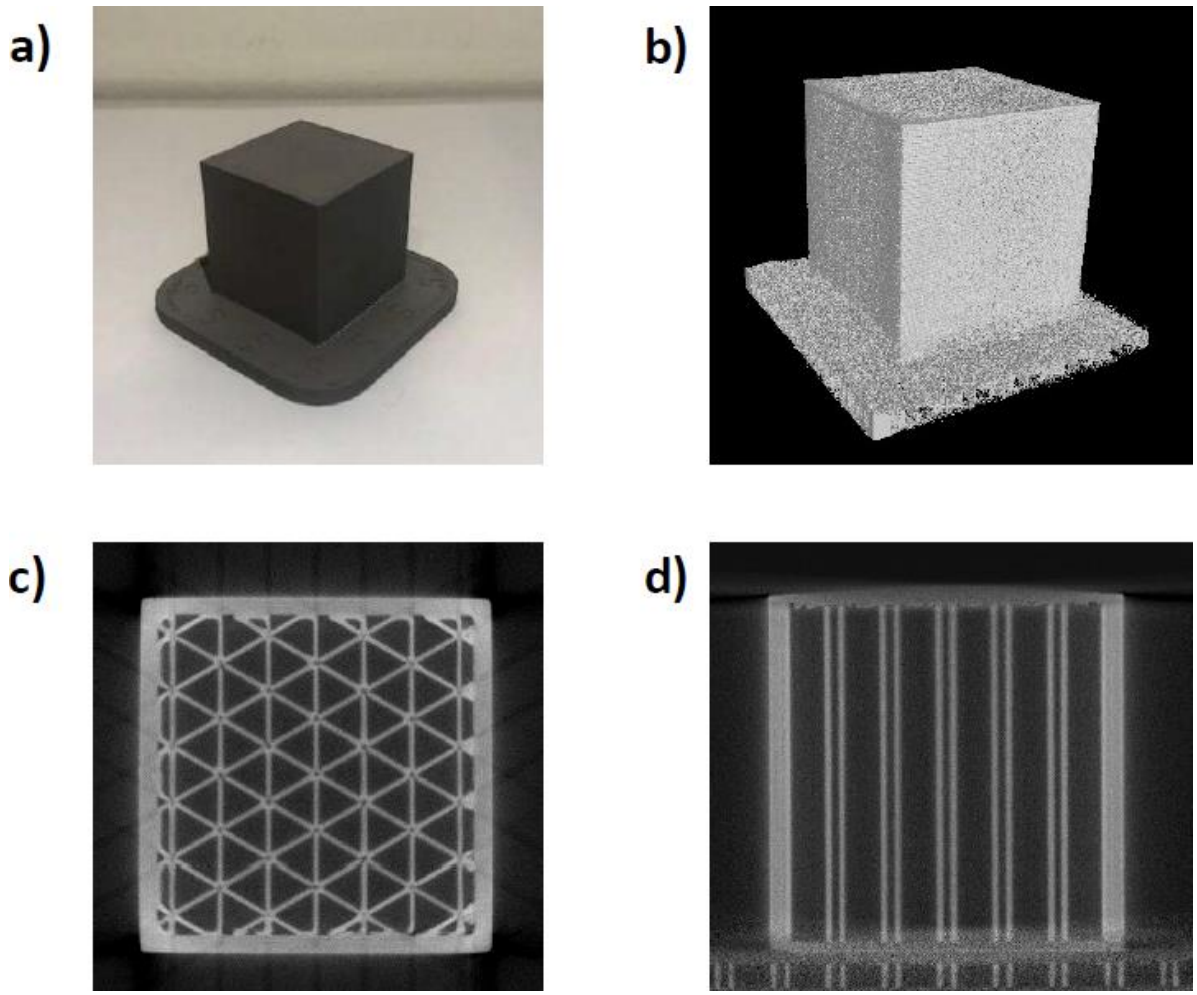

Figure 7 Computed Tomographic Image of a sample with triangular infill pattern. a) Standard image of the sample in isometric view. b) Computed tomographic image of the sample in isometric view. c) Computed tomographic image from the side. d) Computed tomographic image from the top

All the printed samples were scanned via computed tomography. The system used to scan the samples was a Yxlon CT System with a Nikon Microfocus X-Ray machine. The detector is a Perkin Elmer XRD1622 16" x 16" with 200-micron resolution. The samples were scanned at 350kV and 0.5mA. The distance to the object was 325mm and the distance to the detector was 1515mm. This led to a voxel size of 0.0429 mm. An isotropic image of the sample, a top view CT image, and a top view CT image which shows the triangular infill pattern is shown in fig 7. The CT method used in this work clearly shows the internal features of the samples and could be used to compare pre-and post-sintered parts in the future. This would give an idea of the shrinkage behavior for intricate internal geometries, which are often desired from additive manufactured components.

Conclusion

The main aim of the study is to investigate material properties before the sintering stage. A detailed conceptual approach was proposed for this investigation. Cubic samples were manufactured in the Markforged MetalX machine and washed further to remove the binder from the samples. These samples were systematically evaluated for their as-printed characteristics, before the sintering stage. The findings of the current study led to the following conclusions.

- The material composition was similar to 17-4PH steel grade 630 according to XRF results.

- According to measurements, 24.015 mm X 23.801 mm X 23.776 mm, parts were larger than the design after the wash due to the presence of triangular infill strategy, porosity, and loosely packed powder in the cube. The density of the cube was 1.804 g/cm^3.
- The roughness value for the overall surface of the sample was measured as 7.7813 microns. Along and across the valley of the top surface of the samples were 1.5 –1.9 microns and 9 - 12microns.
- The average particle size of the green part was measured to be 2.58 microns in diameter with a standard deviation of 1.23 microns. This measurement was averaged over hundreds of particles from 10 SEM images from 5 different samples.
- CT scan analysis demonstrated the capability to show the internal features of the sample using the equipment and settings we used in this work. The quality of the holes within the part could be documented for comparison with CT scans after sintering. This baseline will enable the estimation of sintering shrinkage for internal and external geometrical features.

Acknowledgment

The authors would like to acknowledge the Siemens Energy doctoral fellowship and the support for coupon manufacturing from Siemens Energy Innovation center, Orlando. The authors express sincere gratitude to Dr. Forrest Ruhge, Mr. Ranier Valentin for their support for manufacturing and CT scanning the samples. Also, the author would like to thank the Material Characterization Facility, AMPAC (Advanced Materials Processing and Analysis Center), CREOL (The College of Optics and Photonics) facilities at UCF for their help in experiments and data collection.

References

[1] Han, Daehoon, and Howon Lee. "Recent advances in multi-material additive manufacturing: Methods and applications." *Current Opinion in Chemical Engineering* 28 (2020): 158-166.
[2] Lewandowski, John J., and Mohsen Seifi. "Metal additive manufacturing: a review of mechanical properties." *Annual review of materials research* 46 (2016): 151-186.
[3] Sames, William J., et al. "The metallurgy and processing science of metal additive manufacturing." *International materials reviews* 61.5 (2016): 315-360.
[4] Frazier, William E. "Metal additive manufacturing: a review." *Journal of Materials Engineering and performance* 23.6 (2014): 1917-1928.
[5] Bandyopadhyay, Amit, and Kellen D. Traxel. "Invited review article: Metal-additive manufacturing—Modeling strategies for application-optimized designs." *Additive manufacturing* 22 (2018): 758-774.
[6] Campbell, Ian, and Terry Wohlers. "Markforged: Taking a different approach to metal Additive Manufacturing." (2017).
[7] Galati, Manuela, and Paolo Minetola. "Analysis of density, roughness, and accuracy of the atomic diffusion additive manufacturing (ADAM) process for metal parts." *Materials* 12.24 (2019): 4122.
[8] Bouaziz, Mohamed Ali, et al. "Microscale mechanical characterization of 17-4PH stainless steel fabricated by Atomic Diffusion Additive Manufacturing (ADAM)." *Procedia Structural Integrity* 28 (2020): 1039-1046.
[9] Yakout, Mostafa, M. A. Elbestawi, and Stephen C. Veldhuis. "A review of metal additive manufacturing technologies." *Solid State Phenomena.* Vol. 278. Trans Tech Publications Ltd, 2018.
[10] Bhavar, Valmik, et al. "A review on powder bed fusion technology of metal additive manufacturing." *Additive manufacturing handbook*. CRC Press, 2017. 251-253.
[11] Tuncer, Nihan, and Animesh Bose. "Solid-state metal additive manufacturing: a review." *Jom* (2020): 1-22.
[12] ASTM," ASTM E122-17 Standard practice for calculating sample size to estimate, with specified precision, the average for a characteristic of a lot of processes", *ASTM International*, 2017, USA.
[13] "Material data sheet- 17-4PH stainless steel", *Marforged*,2020.
[14] ASTM," ASTM A693-16 standard specification for precipitation-hardening stainless and heat-resisting steel plate, sheet and strip", *ASTM International*, 2016, USA.

[15] ASTM," ASTM B311-17 Standard test method for density of powder metallurgy (PM) material containing less than two percent porosity", *ASTM International*, 2017, USA.
[16]ISO, "ISO 25178: Geometrical product specification (GPS)- surface texture: Areal- Part2: terms, definition, and surface texture parameters", *ISO*, 2012, USA.
[17] Rasband, Wayne S. "ImageJ." (1997).
[18] Feret, L. R. La grosseur des grains des matières pulvérulentes. Eidgen. Materialprüfungsanstalt ad Eidgen. Technischen Hochschule, 1930.